JOURNAL OF SOLID STATE CHEMISTRY 37, 204–218 (1981)

Zeolite Structure Type EAB: Crystal Structure and Mechanism for the Topotactic Transformation of the Na,TMA Form

W. M. MEIER AND M. GRONER

Institut für Kristallographie und Petrographie, ETH, Zurich, Switzerland

Received June 23, 1980; in final form September 5, 1980

Synthetic zeolite (Na,TMA)-E represents a new structure type designated EAB. Detailed structure analyses based on X-ray powder diffraction data have been carried out at room temperature, 220°C, and 350°C. The silicate framework, having maximum symmetry $P6_3/mmc$, consists of parallel 6-rings in ABBACC sequence as opposed to AABAAC in erionite (with which it has mistakenly been identified). Large changes in conformation of the EAB framework precede the transformation of (Na,TMA)-E to a sodalite-type product above 360°C. There are also strong indications for this reaction to be topotactic, whereby only one-twelfth of the original siloxane bridges are broken. Details of an acid–base reaction mechanism proceeding in characteristic loops of the structure are discussed. This process brings about the inversion of one-third of the tetrahedra in the silicate framework. The presence of water appears to be essential in this model-type reaction.

Introduction

Solid state transformations of framework silicates involving configurational changes of the anionic network are by no means sufficiently understood. Due to frequent difficulties encountered in experimental studies, e.g., the sluggishness of most of the reactions or the relatively high temperatures required, the reaction paths of these transformations are almost invariably hypothetical. Despite the complexity of their structures, zeolites offer inherent advantages in studies of reaction mechanisms. Structural studies of functional groups in zeolites and reactant states can also be expected to provide a better understanding of structure-stability relationships of widely used zeolitic materials.

Among many examples of zeolites undergoing "reconstructive" phase changes at relatively low temperatures, the transformation of synthetic (Na,TMA)-E[1] at around 360°C to a sodalite-type product appeared particularly suitable for detailed study since crystallinity is essentially retained during reaction. This was already noted by Aiello and Barrer (*1*), who first synthesized the zeolite which was assigned an erionite-type structure on the basis of X-ray powder data. The comparatively low thermal stability of (Na,TMA)-E seems all the more remarkable in view of the considerable stability of acid erionites obtained by deammoniation at elevated temperatures and their wide use as cracking catalysts (*2, 3*).

Our study of (Na,TMA)-E was initiated in particular by "model-reaction" considerations indicating the possibility of a topotactic mechanism involving inversions of aluminosilicate tetrahedra in the framework structure. This paper reports on the chemi-

[1] TMA: Tetramethylammonium.

0022-4596/81/050204-15$02.00/0

cal characteristics and crystal structure of (Na,TMA)-E, including an X-ray study of the transformation reaction.

Synthesis and Characterization of (Na,TMA)-E

Based on the field of formation in the mixed Na,TMA system described by Aiello and Barrer (*1*), optimum conditions for the synthesis of pure (Na,TMA)-E had to be determined first in a series of experiments. It should be noted that a number of other zeolites[2] are also obtained in the same system. The structural purity of the products obtained was carefully evaluated using primarily X-ray powder diffraction patterns from a Nonius–Guinier camera and scanning electron micrographs to detect gel impurities. The following procedure based on mole ratios of

$$3.51\ Na_2O : 3.63\ (Me_4N)_2O : 1.00\ Al_2O_3 : 13.60\ SiO_2 : 372\ H_2O$$

in the reaction system was found to be particularly suitable for the synthesis of (Na,TMA)-E.

A 2.5-m solution of Me_4NOH, filtered through a 0.2-μm Acropor disk is prepared from commercially available Me_4NBr (purum, Fluka) and Ag_2O (puriss., Fluka). The aluminate solution is freshly prepared by dissolving 25.7 g of $NaAlO_2$ in a solution of 27.7 g NaOH in 420 ml of water followed by filtration through a 0.2-μm Acropor filter. One hundred thirty-six grams of precipitated silicic acid (puriss., Fluka) are then stirred up in 420 ml of the 2.5 *M* solution of Me_4NOH for 30 min and 170 ml of water added. The aluminate solution is added at 5°C under intensive stirring. The well-homogenized reaction mixture is then transferred to a steel reactor equipped with stirrer in a water bath at 80°C. Crystallization takes 4 to 5 days, after which about 45 g of the zeolite can be filtered off.

After thorough washing all samples were air-dried at 80°C and then kept in a desiccator at a controlled relative humidity of 52%. Chemical analyses of the samples by atomic absorption (Si,Al), flame spectroscopy (Na), and TGA (H_2O and TMA titrated with sulfamic acid) checked reasonably well but showed in all instances a significant excess of total cation (Na + TMA) in relation to the Al contents. It had to be assumed therefore that the number of water molecules found included a corresponding amount of hydroxyl ions for electroneutrality. The composition of samples GS Lü 63, used in all further work described here, is quite representative and can be given as

$$Na_{8.1}(Me_4N)_{2.2}Al_{9.4}Si_{26.6}O_{72}(OH)_{0.9} \cdot 25\ H_2O,$$

when normalized to 36 Al + Si. The somewhat idealized contents of the unit cell (neglecting OH) of the zeolite could be represented by

$$Na_7(Me_4N)_2Al_9Si_{27}O_{72} \sim 26H_2O.$$

(For comparison, the composition stated by Aiello and Barrer (*1*) for a sample, the preparation of which was not given in detail, is

$$Na_{6.84}(Me_4N)_{3.05}Al_{9.25}Si_{26.75}O_{72} \cdot 17H_2O).$$

X-ray powder data are listed in Table I for the lower angles where overlap is less severe. The *d* spacings given were determined using a Jagozinski focusing camera and silicon as an internal standard. The indexing is based on hexagonal unit cell constants of

$$a = 13.28 \pm 0.01\ \text{Å} \quad \text{and}$$
$$c = 15.21 \pm 0.01\ \text{Å},$$

which were obtained by refinement from 16 nonoverlapping lines. Only indices of lines

[2] Including P(GIS), S(GME), A(LTA), T(SOD), R(FAU), and Ω(MAZ).

which were subsequently found to contribute significantly to composite peaks are listed in Table I. The 320 line at $2\Theta \sim 34°$ for Cu$K\alpha$ was noted to appear unaccountedly in the patterns of some preparations only. It did not show up in the original diffraction pattern of GS Lü 63 but was observed in X-ray patterns taken again of the sample after 2 years. (The line does not occur in the data sets used for the structure analyses reported in this paper). The powder diffraction patterns of (Na,TMA)-E and various forms of erionite match quite well with respect to d spacings but at least a few of the lines at lower angles differ greatly in intensity as can be seen by comparing patterns (a) and (b) in Fig. 1. The strongest line of erionite, the 100 at $2\Theta \sim 7.5°$ for Cu$K\alpha$, just barely shows up in the pattern of (Na,TMA)-E.

(Na,TMA)-E forms plate-like crystals which are invariably twinned. Figure 2 shows a scanning electron micrograph of a typical sample, the crystallite size being around 1 or 2 μm. The rosette-like aggregates resemble synthetic zeolite losod (*4*) in

TABLE I

d SPACINGS (IN Å) AND RELATIVE INTENSITIES OF (Na,TMA)-E AT ROOM TEMPERATURE

hkl	I_{obs}	d_{obs}	d_{calc}	*hkl*	I_{obs}	d_{obs}	d_{calc}	*hkl*	I_{obs}	d_{obs}	d_{calc}
100	2	11.58	11.50	311	5	3.120	3.122	332	10	2.121	2.125
								306			2.115
101	78	9.20	9.17	303	3	3.072	3.058	512	4	1.994	1.993
002	17	7.63	7.61	222	2	3.053	3.042	504	3	1.969	1.968
110	56	6.65	6.64	105	23	2.942	2.941	600	1	1.901	1.902
102	18	6.30	6.34	400	9	2.876	2.875	334	3	(1.915)	1.913
200	1	5.77	5.75	214	31	2.863	2.862	513			
201	18	5.36	5.38	401	58	2.825	2.825	008	6	1.901	1.901
112	2	5.018	5.002	304	1	2.704	2.700	601			
				313							
103	2	4.650	4.640					520	12	1.842	1.842
202	38	4.588	4.587	205	20	2.691	2.689	505			1.835
				402				432			1.835
210	5	4.341	4.346					118			1.828
				[a]320	(15)	2.642	2.638				
211	59	4.176	4.179					416	18	1.785	1.784
				410			2.510				
300	35	3.842	3.833	224	19	2.506	2.501	218	1	1.743	1.742
				403			2.501	611			
203	3	3.792	3.803								
004				215	6	2.492	2.493	612	3	1.709	1.709
				322			2.492				
212	100	3.776	3.774					109	1	1.672	1.672
301	1	3.716	3.717	106	5	2.475	2.476	336	20	1.660	1.667
				411				440			1.660
104	64	3.616	3.611					524			1.657
302	2	3.425	3.423	314	2	2.438	2.444	620	9	1.593	1.595
				412	1	(2.385)	2.383	614			1.592
220	20	3.320	3.320	323	3	2.342	2.341				
114			3.300					219	1	(1.575)	1.575
213			3.300	413	4	2.253	2.249	622	3	1.561	1.561
310	2	3.190	3.189	330	10	2.214	2.213	606	4	1.529	1.529
204	13	3.181	3.172								

[a] Absent in the patterns of some preparations.

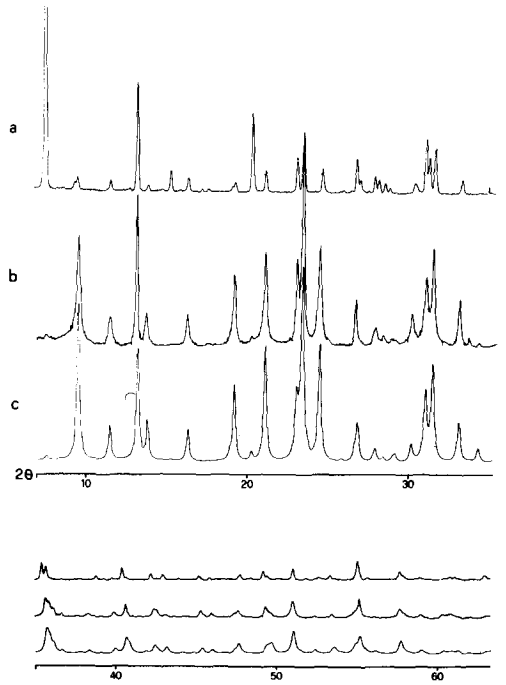

FIG. 1. Observed X-ray powder patterns of natural erionite (a) from Pine Valley, Nevada, and (Na,TMA)-E (b) compared with calculated pattern of EAB-type structure (c).

morphology and are quite unlike normal erionite, which tends to form rods or needles.

The irreversible transformation to a sodalite-type phase at around 360°C is clearly discernible in powder diffraction patterns of (Na,TMA)-E recorded as a function of temperature with the aid of a Lenné camera. As can be seen from the pattern shown in Fig. 3, the transformation is preceded by substantial changes of the lattice constants and there is no apparent loss in crystallinity prior to the reaction. According to our thermoanalytical data (Fig. 4) the changes in cell dimensions up to about 250°C must be primarily attributed to the first stage of dehydration, as revealed by TGA in combination with mass spectrometry. (It must be noted that the temperature scales in Figs. 3 and 4 cannot be directly related because of considerable differences in heating rates).

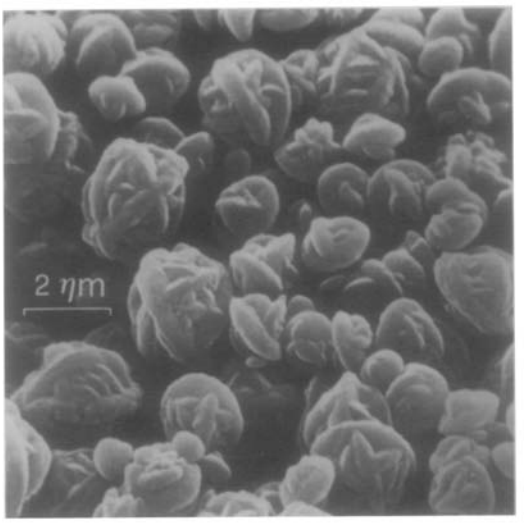

FIG. 2. Scanning electron micrograph of (Na,TMA)-E as synthesized.

The decomposition of the organic cation sets in somewhat below 350°C and is accompanied by further release of water which becomes very noticeable around or just above the transition temperature. Scanning electron micrographs of the cubic reaction product reveal no significant changes in morphology as compared to the parent material. The sodalite-type product is clearly pseudomorphic.

Most of the Na ions in (Na,TMA)-E, i.e., over seven per unit cell, could be readily exchanged by treating the zeolite with a solution of 1 *M* KCl at 80°C. It is very

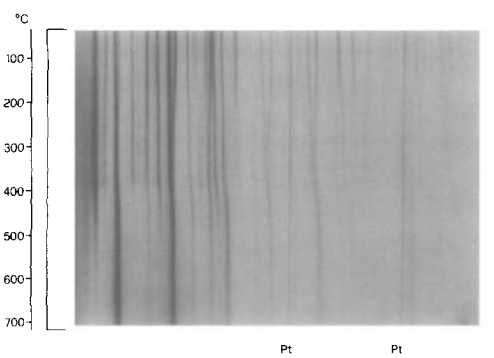

FIG. 3. Lenné photograph of (Na,TMA)-E heated in ordinary air at a rate of 0.5°C per minute.

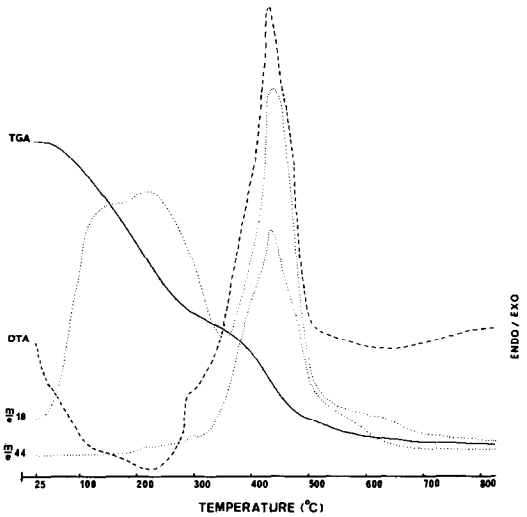

FIG. 4. Thermal analysis of (Na,TMA)-E with Mettler thermoanalyzer. DTA and TGA coupled with mass spectrometric detection of H_2O and CO_2 formed. Sample heated in air at a rate of 10°C per minute.

noteworthy that, unlike the Na form, (K,TMA)-E obtained in this way does *not* transform into a sodalite-type product on heating. As revealed by the Lenné photograph shown in Fig. 5, (K,TMA)-E is apparently stable up to temperatures of over 500°C and the changes of the cell dimensions on heating are much less pronounced than those of (Na, TMA)-E.

Structure Analyses

All structural work on (NA,TMA)-E reported here had to be done with X-ray powder data. Intensity values were obtained with PAD-1, a computer-controlled X-ray powder diffractometer specially developed for the measurement of accurate data for structure analyses (*5*). No preferred orientation effects were encountered in the flat samples used. Room temperature data were collected with monochromatized Cu$K\alpha$ radiation in the 2Θ range 7–100°. Complete data sets were also obtained for 2Θ up to 65° at temperatures of 220, 350, and 490°C, using a furnace with appropriate temperature control. The sample in the furnace was passed by a slow stream of nitrogen. The data collection at elevated temperatures took around 7 hr for each set. At each temperature a standard reflection was measured periodically. Further experimental details and powder patterns recorded at different temperatures are given in the thesis by Groner (*6*). Partially overlapping peaks were resolved with the aid of the program CUFIT (*7*) and the usual data reduction procedures were applied. The total number of nonzero intensity values which could be measured in this way was 77 at room temperature, 44 each at 220 and 350°C, and 18 at 490°C.

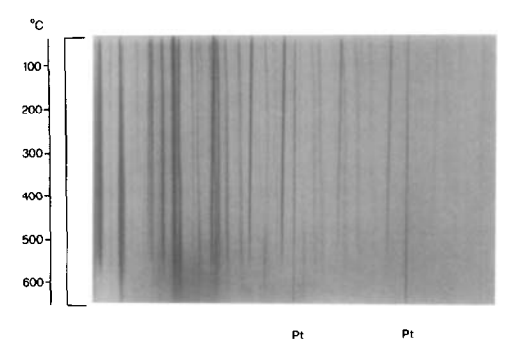

FIG. 5. Lenné photograph of (K_{ex},TMA)-E heated in ordinary air at a rate of 0.5°C per minute.

The evidence of hexagonal symmetry and unit cell constants of $a = 13.28$ and $c = 15.21$ Å was considered to be a strong indication for supposing that the framework structure is made up of parallel 6-rings stacked to form a period comprising six layers. There are 10 possible stacking sequences for this period if both single and double 6-rings are considered. These 10 structures are presented in Table II. Three of these have previously been reported to occur in zeolites, the structure type of chabazite (CHA), of erionite (ERI), and of liottite (LIO). The value of $c/a = 1.146$ observed for (Na,TMA)-E at room temperature would indicate the presence of two double 6-rings in the sequence (Nos. 6–9) according to the predicted values based on DLS calculations (*8*) listed in Table II. The

TABLE II

POSSIBLE SEQUENCES OF 6-RINGS FOR $c \sim 15$ Å (PERIOD OF SIX LAYERS)

No.	Sequence	No. of double rings	Maximum symmetry	Theoretical c/a (8)	Observed structure type[a]
1	ABCACB	0	$P6_3/mmc$	1.203	—
2	ABABAC	0	$P\bar{6}mc$	1.236	LIO
3	AABABC	1	$P3ml$	1.194	—
4	AABACB	1	$P3ml$	1.210	—
5	AABCBC	1	$P\bar{3}ml$	1.215	—
6	AABAAC	2	$P6_3/mmc$	1.163	ERI
7	AABBAB	2	$P3ml$	1.195	—
8	AABBCB	2	$P3ml$	1.190	—
9	ABBACC[b]	2	$P6_3/mmc$	1.140	EAB
10	AABBCC	3	$R\bar{3}m$	1.087	CHA

[a] See (9) for zeolite structure-type designations and further references on known zeolite structures.

[b] AABCCB in lexicographical setting otherwise used in this table. ABBACC has been given preference in this paper for reasons of convenience.

theoretical ratios agreeing best with the observed c/a are those for Nos. 9 and 6. Nevertheless, plots of theoretical powder patterns were computed for all 10 sequences listed using optimized coordinates obtained by DLS (*10*). Visual comparison of these plots with diffractometer patterns showed that all sequences except Nos. 4, 6 (ERI), and 9 could be excluded from further consideration. AABACB (No. 4) and AABCCB (No. 9 in comparable setting) differ in one layer only. Also, of all 10 structures listed, No. 4 is the most closely related to the sequence in the sodalite-type reaction product deviating by only one out of six layers (AABACB instead of ACBACB in comparable setting).

$R(I)$ values[3] calculated for the three trial structures using the first 30 lines of the diffraction pattern at room temperature were found to be

0.90 for AABACB (No. 4),
0.75 for AABAAC (No. 6),
0.53 for ABBACC (No. 9).

This showed, as suspected earlier, that the framework structure of (Na,TMA)-E is not of the erionite type. The sequence ABBACC was consequently adopted for further testing and refining of the structure at room temperature. Coordinates of the framework atoms computed by DLS assuming uniform Si,Al–O distances of 1.64 Å were used to start with. DLS calculations also served as a test that space group $P6_3/mmc$ could be chosen without imposing inexpedient geometrical constraints on the framework (also taking into account the limited resolution allowed by the available data). All subsequent work reported in this paper is based on space group $P6_3/mmc$.

An initial three-dimensional Fourier map of the room temperature structure computed from the first 30 lines of the data set revealed most of the cation and water positions, besides confirming the positioning of the framework atoms. Apart from Fourier maps structure refinement was largely based on least-squares refinement using a modified program version of ORFLS (by Busing, Martin, and Levy) adapted for powder data by Baerlocher (*11*). Assumptions regarding the distribution of the cations and water molecules (which might have biased the outcome of the structure

[3] Defined at $R(I) = \Sigma|I_0 - I_c|/\Sigma I_0$, where $I_c = \Sigma m_i F_{c,i}^2$, m_i being the multiplicity.

refinement) were deliberately avoided. Therefore scattering factors of oxygen atoms combined with occupancy parameters were used for all nonframework sites throughout the refinement. Similarly scattering factors of Si were applied for all T atoms (Si,Al). Initial refinement of the structure was carried out using the first 30 lines only. The refinement process was extended to include all the 77 intensities after all atom sites had been sufficiently well established. A total of seven significant nonframework sites could be located and the sum of the electrons eventually accounted for in the structure analysis was noted to correspond with that of the chemical composition within 1%. The final $R(I)$ value of the room temperature structure was 0.178. The observed and calculated powder patterns of (Na,TMA)-E using final parameters are shown for comparison in Fig. 1. Observed and calculated intensity values determined at room temperature, 220°C, and 350°C are available (*6*).

The structure analysis at 220°C was started with the first 25 lines and the coordinates of the framework atoms determined at room temperature which gave an $R(I)$ value of 0.56. Refinement of the structure was basically carried out in the same way as at room temperature except that soft constraints were introduced with respect to the T–O distances in the framework. Some eight nonframework sites could be located with confidence but the temperature parameters of the atoms in these sites had to be replaced by a constant average value to keep the number of variables within reasonable limits. Refinement including all 44 intensities finally reduced the $R(I)$ value to 0.191 (or 0.141 for the first 28 lines).

Refinement of the structure at 350°C was conducted in the same manner. The nonframework atoms could be assigned individual temperature factors in view of the smaller number of parameters. The most conspicuous peak in the Fourier maps, showing up immediately, was that of site III. The final $R(I)$ value recorded for all 44 intensity data was 0.197.

The observed intensity data at 490°C were found to agree quite well with those of synthetic hydroxy sodalite. The diffraction pattern could be readily indexed on the basis of a body-centered cubic lattice having a unit cell constant a of 8.948(5) Å. Further evidence that the structure of the reaction product at 490°C is indeed of the sodalite type was obtained by a Fourier map computed from the 18 intensities measured. Moreover, a few refinement cycles assuming space group $I\bar{4}3m$ produced reasonable positional and temperature parameters (*6*). The structure analysis of the sodalite-type product was not continued beyond this stage, however, because of insufficient data for more extensive refinement at lower symmetry.

Results and Discussion of the EAB-Type Structure

Unit cell constants of (Na,TMA)-E at the temperatures of our structural studies are given in Table III. Final parameters of the framework atoms at 20, 220, and 350°C are listed in Table IV and those of the nonframework sites in Table V. Particularly relevant interatomic distances of the structure at room temperature are assembled in Table VI.

TABLE III

HEXAGONAL UNIT CELL CONSTANTS (±0.01 Å) OF (Na,TMA)-E AT DIFFERENT TEMPERATURES

Temperature (°C)	a (Å)	c (Å)
20	13.28	15.21
220	13.00	15.47
350	12.86	15.51
490	(12.65)	(15.50)[a]

[a] Values calculated from a = 8.948 Å of the cubic sodalite-type product.

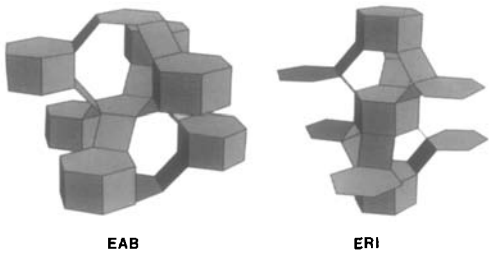

FIG. 6. Skeletal diagrams of EAB and ERI frameworks (with 6-ring sequences ABBACC and AABAAC).

The framework structure of (Na,TMA)-E defines a new zeolite structure type, designated EAB in recognition of the first reported synthesis of this synthetic zeolite by Aiello and Barrer (*1*). EAB is closely related to the structure type of erionite, ERI, and belongs to the chabazite family of zeolite structures comprising frameworks made up of parallel single and/or double 6-rings of *T* atoms.

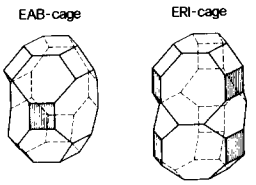

FIG. 7. Large cage in EAB and ERI (*8*).

The relationship of EAB and ERI is depicted in Fig. 6, showing the sequences ABBACC and AABAAC. It should be mentioned that the sequence ABBACC found in EAB-type structures was also considered as a possibility by Staples and Gard in their determination of the erionite structure (*12*) which was later confirmed by detailed refinement (*13*). Either of the two structure types can be transformed into the other simply by interchanging single and double rings.

This more formal relationship between

TABLE IV

REFINED ATOMIC COORDINATES AND THERMAL PARAMETERS OF THE FRAMEWORK ATOMS OF (Na,TMA)-E AT ROOM TEMPERATURE, 220°C, AND 350°C[a]

Atom	Position	*x*	*y*	*z*	*B* (Å²)
*T*1	12*i* (2)	0.233(2)	0	0	0.9
		0.249(4)	0	0	1.0
		0.249(5)	0	0	0.8
*T*2	24*l* (1)	0.425(2)	0.093(2)	0.146(1)	2.4
		0.430(4)	0.088(7)	0.150(5)	2.4
		0.426(4)	0.086(4)	0.153(4)	4.1
O1	24*l* (1)	0.309(2)	−0.003(2)	0.088(2)	0.8
		0.305(5)	−0.008(6)	0.087(5)	3.1
		0.325(7)	0.005(9)	0.082(5)	4.8
O2	12*k* (*m*)	0.212(2)	0.106(1)	0.006(4)	0.5
		0.202(8)	0.101(4)	−0.026(9)	3.1
		0.214(6)	0.107(3)	0.011(8)	0.8
O3	12*k* (*m*)	0.478(2)	0.239(1)	0.117(3)	3.2
		0.406(4)	0.203(2)	0.150(5)	3.1
		0.428(6)	0.214(3)	0.162(6)	5.8
O4	12*j* (*m*)	0.399(3)	0.081(4)	¼	2.6
		0.375(6)	0.014(5)	¼	3.1
		0.373(8)	0.009(4)	¼	2.9
O5	12*k* (*m*)	0.536(2)	0.072(4)	0.106(3)	2.0
		0.545(3)	0.090(6)	0.109(5)	3.1
		0.576(4)	0.152(8)	0.127(7)	5.5

[a] Based on space group $P6_3/mmc$ (with estimated standard deviations in parentheses).

TABLE V

POSITIONAL, POPULATION, AND THERMAL PARAMETERS OF NONFRAMEWORK SITES IN (Na,TMA)-E

Site	Position	Occupancy[a]	x	y	z	B (Å^2)
			(a) At room temperature			
I	4*f* (3*m*)	0.87(6)	$\frac{2}{3}$	$\frac{1}{3}$	−0.003(10)	5.0
II	6*h* (*mm*)	0.50(4)	0.461(4)	−0.078(8)	$\frac{1}{4}$	2.0
III	12*k* (*m*)	0.91(12)	0.454(6)	0.227(3)	−0.122(5)	5.0
IV	4*e* (3*m*)	1.19(6)	0	0	−0.184(4)	0.6
V	6*h* (*mm*)	0.70(4)	0.068(4)	0.136(8)	$\frac{3}{4}$	0.9
VI	6*h* (*mm*)	1.21(5)	0.350(6)	0.175(3)	$\frac{3}{4}$	5.0
VII	12*k* (*m*)	0.49(2)	0.708(8)	0.354(4)	−0.073(7)	2.1
			(b) At 220°C			
I	4*f* (3*m*)	0.92(8)	$\frac{2}{3}$	$\frac{1}{3}$	0.048(15)	3.9
II	12*k* (*m*)	0.20(7)	0.438(15)	−0.124(30)	0.163(30)	3.9
III	12*k* (*m*)	0.87(6)	0.440(12)	0.220(6)	−0.156(12)	3.9
IV	4*e* (3*m*)	0.60(8)	0	0	−0.221(20)	3.9
V	12*k* (*m*)	0.58(3)	0.136(12)	0.068(6)	−0.220(10)	3.9
VIII	4*e* (3*m*)	0.46(9)	0	0	−0.073(15)	3.9
IX	12*k* (*m*)	0.56(6)	0.404(10)	−0.192(5)	−0.057(15)	3.9
X	6*h* (*mm*)	0.52(7)	0.758(12)	0.379(6)	$\frac{1}{4}$	3.9
			(c) At 350°C			
I	4*f* (3*m*)	1.14(9)	$\frac{2}{3}$	$\frac{1}{3}$	0.135(10)	5.3
II	12*k* (*m*)	0.80(6)	0.412(4)	−0.176(8)	0.159(10)	4.0
III	12*k* (*m*)	0.86(6)	0.372(3)	0.186(6)	−0.162(10)	1.1
IV	4*e* (3*m*)	1.38(9)	0	0	−0.114(8)	1.3
XI	12*k* (*m*)	0.74(5)	0.536(8)	0.268(4)	−0.107(10)	4.9

[a] Based on oxygen scattering factors (eight electrons).

EAB and ERI is contrasted by the complete difference with respect to the cages present (apart from the hexagonal prism). The smaller cages (easily discernible in Fig. 6) which are associated with cation specificity are gmelinite-type (TMA,Na) in EAB and cancrinite-type cages (K) in ERI. The larger cages (Fig. 7) in the two structure types differ also appreciably.

Assuming an oxygen radius of 1.35 Å the crystallographic free diameter defined by the boat-shaped 8-rings of the gmelinite cages are 3.7 × 4.8 Å in (Na,TMA)-E at room temperature. These pore dimensions are just about the same as those of erionite. More pronounced diffusion constraints are to be expected in EAB, however, for in the latter there is no direct access from one large cage to another (as in erionite). In EAB the channel system is two-dimensional and molecules which cannot pass through a 6-ring have to traverse a gmelinite cage on their way from one large cage to another.

Our structure analyses of (Na,TMA)-E indicate that EAB is a relatively nonrigid type of framework. The conformational changes of the silicate framework recorded on heating and dehydration are very pronounced as illustrated in Fig. 8. These marked changes in conformation are reflected in the substantial changes of the unit cell dimensions which were also noticed previously (*1*).

Moderately precise interatomic distances could only be obtained at room temperature

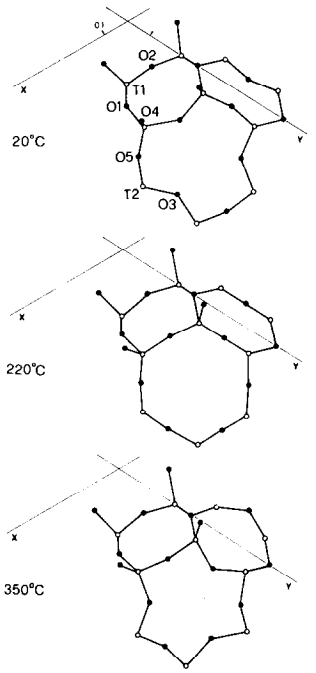

FIG. 8. Conformational changes in framework structure of (Na,TMA)-E on heating.

TABLE VI

INTERATOMIC DISTANCES (IN Å) OF (Na,TMA)-E AT ROOM TEMPERATURE[a]

	*T*1–O1	1.69(2×)	*T*2–O1	1.68	
	*T*1–O2	1.57(2×)	*T*2–O3	1.76	
			*T*2–O4	1.61	
			*T*2–O5	1.74	
	mean	1.63	mean	1.70	
I–O3	2.84(3×)	III–O1	2.66	V–O4	3.40
I–O5	3.44(2×)	III–O2	3.41	V–IV	1.87(2×)
I–III	3.05(3×)	III–I	3.05	V–V′	2.73(4×)
I–VII	1.17(3×)	III–II	3.35		
		III–VI	2.29	VI–O1	3.24(2×)
		III–VII	2.37(2×)	VI–O4	3.21
		III–VII′	3.01	VI–II	3.35
II–O4	2.62(2×)			VI–III	2.28(2×)
II–O5	2.79(2×)				
II–T2	2.99(4×)			VII–I	1.17
II–III	3.35	IV–IV′	2.01	VII–III	2.36(2×)
II–VI	3.35(4×)	IV–V	1.87(6×)	VII–III′	3.01

[a] Estimated standard deviations are about 0.03 Å for *T*–O bond lengths and at least 0.10 Å for distances involving nonframework sites. Distances for the latter are listed up to 3.5 Å.

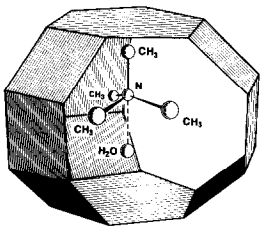

FIG. 9. Location of Me_4N^+ in gmelinite cage of (Na,TMA)-E.

(the standard deviations at elevated temperatures being at least three times as high). The *T*–O distances observed in (Na,TMA)-E generally decrease as expected with increasing *T*–O–*T* angles which range from 129 to 159° at room temperature. Averaged *T*–O distances were found to agree remarkably well with predicted values based on composition. The mean values of 1.63 Å for *T*1–O (1.66 Å at 220°C; 1.62 Å at 350°C) and 1.70 Å for *T*2–O (1.71 Å at 220°C; 1.68 Å at 350°C) are a good indication that most if not all the Al atoms are located in the double 6-rings (consisting of *T*2 atoms). The single 6-rings (made up of *T*1 atoms) could quite possibly contain Si only.

The unequivocal assignment of cations and water molecules to the located sites is complicated by the high space group symmetry, which does not apply to the actual arrangement of the nonframework atoms (nor to the Si,Al distribution), but had to be used in the structure refinement to keep the number of parameters within acceptable limits. Thus, the Fourier peak observed at site IV inside the gmelinite cage results from the superposition (due to the mirror at $z = \frac{3}{4}$) of a nitrogen atom of TMA and a water molecule. Figure 9 shows the arrangement deduced of the TMA and water molecule in the gmelinite cage. Site V at $z = \frac{3}{4}$ accommodates three of the four methyl groups of the TMA. The apparent discrepancy of the distance between IV and V of around 1.87 Å and the expected N–C bond length of 1.48 Å can be accounted for by considering the effects of the assumed sym-

metry and the large standard deviations. For symmetry reasons again the fourth methyl group could not be observed since the expected peak would amount to no more than $\frac{1}{2}$ C atom or 3 electrons only. Site I in the large cage, just above and below the double 6-rings, also appears to be the result of a symmetrization effect. Bearing in mind the limited resolution site I is best considered jointly with the neighboring site VII. The total occupancy of these two sites amounts to about 19 electrons at room temperature (diminishing to around 9 electrons at 350°C). Based on coordination and interatomic distances at room temperature the contents of sites I and VII are likely to consist of sodium ions and water molecules in about equal numbers. Site I is primarily coordinated by three framework oxygens O3 and by three type III sites forming roughly a trigonal prism. Site II, facing 4-rings of the hexagonal prism, seems to be partially occupied by water molecules at room temperature. There are strong indications that site III in the large cage near the 8-ring is a practically fully occupied water position playing an essential role in the transformation reaction to the sodalite-type structure as discussed in the next section. Finally, site VI which is nearest to the center of the 8-ring could contain either sodium ions or water. It is no longer occupied at elevated temperatures and whatever sodium ions happen to be in site VI at room temperature seem to move into site II at higher temperatures. In line with additional criteria, including charge distribution and comparison with other structures, the various sites could consequently accommodate about the following numbers of cations and water molecules at room temperature (in round numbers per unit cell):

I + VII	4 Na + 4 H_2O
II	3 H_2O
III	12 H_2O
IV	2 H_2O + 2 N
V	(6 CH_3 belonging to TMA)
VI	4 Na + 2 H_2O.

The location of the single hydroxyl ion cannot be inferred on the basis of the available results.

It is significant that the two gmelinite cages per unit cell in (Na,TMA)-E are both occupied by a TMA cation (as shown in Fig. 9) which provides further evidence for the cation specificity of this cage (*14*) and possible template effects (*15*). Apart from gmelinite cages, TMA cations have been located in sodalite- (*16*) and in gismondine-type cages (*11*) all of which are about equal in size. Remarkably, every one of the zeolites which were reported to crystallize in the Na,TMA system (*1*) contain one of these cage types, i.e., gmelinite-type (species E, S, Ω), sodalite-type (A, R, T), and gismondine-type cages (P). The zeolites containing sodalite- and gismondine-type cages are also obtained in the monocationic Na system. TMA plays a structure-directing role in the formation of gmelinite cages occurring in EAB-, GME-, MAZ-, and OFF-type zeolite structures. (The latter forms in the binary K,TMA system and contains K-selective cancrinite-type besides gmelinite-type cages).

Mechanism of the Transformation of (Na, TMA)-E

When (Na,TMA)-E transforms into a sodalite-type product above 360°C the stacking sequence of the 6-rings in the EAB-type structure changes according to the scheme

A B B A C C
↓ ↓
A B C A B C.

Since two-thirds of the layers remain unaffected on this ground and in view of the pseudomorphic product, the reaction is conceivably topotactic in nature.

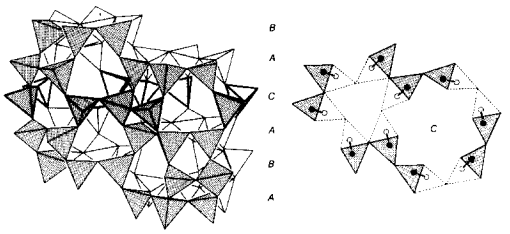

FIG. 10. Framework structure of losod (left) and slightly idealized inversion scheme of tetrahedra in C layer leading to C → B (from *17*).

Transformation reactions in framework silicates involving a change in the stacking sequence are by no means uncommon. Synthetic zeolite Li-losod, with stacking sequence ABAC of 6-rings, transforms into Li-cancrinite based on ABAB stacking when contacted with dilute LiOH solution (*4*). Various considerations have given rise to the postulate that the process requiring minimal reconstructive changes in the Si, Al–O bonding scheme must be a cooperative inversion-type mechanism illustrated in Fig. 10 for the losod → cancrinite reaction

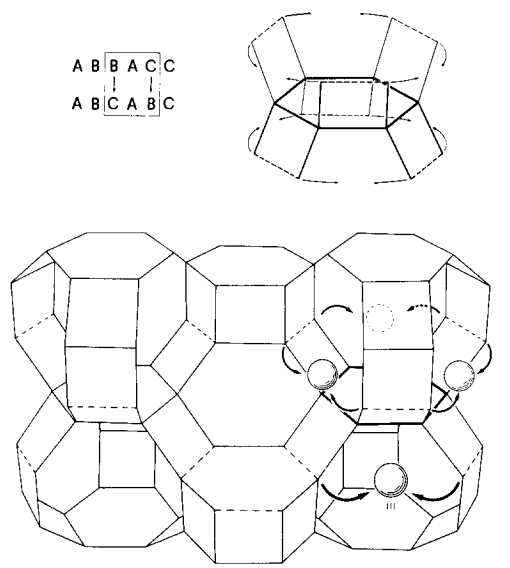

FIG. 11. Reaction loops in EAB framework undergoing transformation to sodalite-type structure. Disrupted *T*–O–*T* bridges are marked by dashed lines and water positions in site III are indicated by spheres.

(*17*). The particular inversion in losod was thought to be brought about by a nucleophilic substitution reaction with Si and Al being attacked by hydroxyl ions and going through a 5-coordinated transition state. Similar inversions have been postulated repeatedly for other silicate types (notably ortho and chain silicates) ever since Taylor and co-workers introduced the concept in terms of "filled-empty tetrahedron migration" assuming the process to be catalyzed by water (*18–20*).

If the reaction of (Na,TMA)-E is interpreted in terms of an inversion-type process then only $\frac{1}{12}$ of the *T*–O–*T* bridges present in the EAB framework need to be broken. These are indicated by dashed lines in Fig. 11. All the other *T*–O–*T* bridges are retained, thus preserving the connectivity of the silicate network to a large extent.

The proposed reaction scheme is a two-stage process taking place in closed loops outlined in Fig. 11. A reaction loop comprises the *T* atoms in the B and C layers which are directly connected to a single 6-ring. There is one such reaction loop per unit cell. The transformation reaction is intimately associated with the decomposition of the two TMA cations per unit cell. It appears unlikely that the reaction is set off by the hydroxyl ion supposed to be present at room temperature since the transformation would then have to set in prior to the formation of protons formed by thermal decomposition of the TMA cations. The decomposition of the quaternary ammonium ion was noted to start around 300°C. The proton supplied by the first TMA on decomposition is presumably neutralized by the hydroxyl group and the actual transformation reaction is thus delayed. This reaction sets in when additional protons become available in the course of further decomposition of TMA. The protolytic breakup of the *T*–O–*T* bridges is initiated by a single proton per loop. The mechanism of this first reaction stage, the hydroxyl-

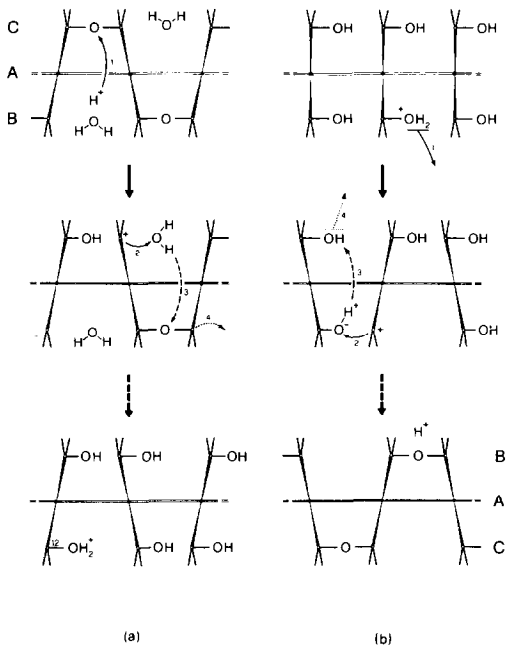

FIG. 12. Reaction steps of two-stage process in reaction loop of (Na,TMA)-E transforming to sodalite-type product. Hydroxylation (a) and ring closure stage (b).

ation stage, is indicated in Fig. 12a. The initial proton gives rise to a hydroxyl group and a 3-coordinate T atom which, being a Lewis acid site, then reacts with the adjacent water molecule (in site III). This sets free a proton again which then attacks the next T–O–T bridge just below (or above) etc. This reaction proceeds around the loop and the product of this first reaction stage is a set of 12 hydroxylated T atoms in the loop as well as a remaining proton. It is noteworthy that the T–O–T bridges involved in the reaction all consist of $T2$ sites occupied in part by Al while the unaffected single 6-ring is composed of $T1$ atoms (Si).

The second stage of the proposed reaction scheme (shown in Fig. 12b), the ring closure or dehydroxylation stage, is activated by dehydration leaving again a 3-coordinate T site. A new T–O–T bridge is then formed by reaction of this Lewis acid site with the nearby hydroxyl group. The proton thus produced combines with the next hydroxyl group giving rise to further dehydration. This repeats around the loop (in the direction opposite to the sequence in the hydroxylation stage). The net result of the two-stage reaction is a set of inverted tetrahedra.

A necessary requirement for this second reaction sequence, the ring closure stage, to take place is a considerable conformational change such that the hydroxyl groups can react with the acid T sites. The observed changes in conformation (Fig. 8) provide actual supporting evidence for this. It must be presumed that the zeolite framework becomes even more flexible in the less constrained hydroxylated state. According to this scheme, protons act as catalysts in this transformation reaction and the presence of water (in site III) is essential for complete hydroxylation in the first stage. Figure 13 illustrates how site III shows up even in low-resolution Fourier sections and how this water molecule is drawing nearer to the required position as the transition temperature is approached.

The observation that (Na,TMA)-E no

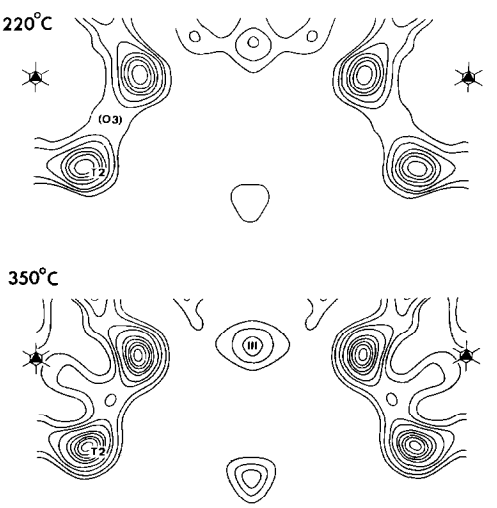

FIG. 13. Fourier sections (for $z = 0.154$) computed from observed powder diffraction intensities showing site III at 220 and 350°C.

longer undergoes the transformation after potassium exchange cannot be fully explained yet. The comparatively small changes in the cell dimensions of (K, TMA)-E with temperature (noticeable on comparison of Figs. 3 and 5) seem to indicate that conformational changes of the EAB framework are minor in the presence of potassium ions. This could well prevent the ring closure in the reaction scheme. Potassium ions were found to be responsible for the remarkable thermal stability of clinoptilolite where these ions were located in the 8-rings of the structure (*21*). A potassium ion in the comparable 8-ring of the EAB framework structure could in fact rule out occupancy of the nearby site III by water and thus effectively prevent the reaction according to the scheme. Further structural investigations are necessary to elucidate these and other possibilities. Additional information is also expected from studies in progress of other members of the chabazite family.

Conclusions

The synthetic zeolite characterized in this paper represents a new structure type, designated EAB, differing from that of erionite (ERI). It provides a further example (e.g., to that of zeolite P) demonstrating that even *close similarity* in powder diffraction patterns is not enough to assign a zeolite structure type, excepting very favorable cases. The chemical properties of this synthetic zeolite, including the conditions of formation and solid state transformation, are also such that it should no longer be confused with erionite.

This synthetic zeolite and related phases provide convenient model systems for direct investigations of the role of water and protons in solid state reactions of silicates. Mechanistic considerations outlined in this paper also show how inversions of tetrahedra in such processes can be related to acid–base reactions in the presence of water.

Acknowledgments

Helpful discussions with Dr. Ch. Baerlocher and with Dr. G. T. Kerr are gratefully acknowledged. Thanks are also due to Mrs. B. Luethi, S. Cartlidge, A. Hepp, Ms. E. Keller, and H. Rechsteiner for practical assistance; to Dr. J. R. Guenter for useful advice; and to P. Waegli for supplying scanning electron micrographs. This study was supported by a grant from the Swiss National Science Foundation.

Note Added in Proof: More recent studies by S. Cartlidge, G. T. Kerr and W. M. Meier (to be published) have shown that the EAB-type structure is retained on calcination of (Na,TMA)-E in *dry air*. Also, TMA plays little or no role in the topotactic transformation.

References

1. R. Aiello and R. M. Barrer, *J. Chem. Soc. A*, 1470 (1970).
2. N. Y. Chen and W. E. Garwood, *Adv. Chem. Ser.* **121**, 575 (1973).
3. T. J. Weeks Jr., C. L. Angell, and A. P. Bolton, *J. Catal.* **38**, 461 (1975).
4. W. Sieber and W. M. Meier, *Helv. Chim. Acta* **57**, 1533 (1974).
5. Ch. Baerlocher and H. Moeck, *Acta Crystallogr. Sect. A* **31** (Suppl.), 237 (1975).
6. M. Groner, Doctoral Thesis No. 6368, ETH Zurich (1979).
7. W. Thoeni, "CUFIT, a FORTRAN Program for the Parametrization of a Measured Profile by the Method of Least Squares." Institute of Crystallography, ETH Zurich (1972).
8. H. Rechsteiner and W. M. Meier, to be published.
9. W. M. Meier and D. H. Olson, "Atlas of Zeolite Structure Types," International Zeolite Association (1978).
10. Ch. Baerlocher, A. Hepp, and W. M. Meier, "DLS-76: A Program for the Simulation of Crystal Structures by Geometric Refinement." Institute of Crystallography, ETH Zurich (1978).
11. Ch. Baerlocher and W. M. Meier, *Helv. Chim. Acta* **53**, 1285 (1970).
12. L. W. Staples and J. A. Gard, *Mineral. Mag.* **32**, 261 (1959).

13. A. KAWAHARA AND H. CURIEN, *Bull. Soc. Chim. Fr.* **92,** 250 (1969).
14. E. FLANIGEN, *Adv. Chem. Ser.* **121,** 119 (1973).
15. L. D. ROLLMANN, *Adv. Chem. Ser.* **173,** 387 (1979).
16. Ch. BAERLOCHER AND W. M. MEIER, *Helv. Chim. Acta* **52,** 1853 (1969).
17. Ch. BAERLOCHER, M. GRONER, AND W. M. MEIER, "Fourth European Crystallographic Meeting, Oxford, Collected Abstracts A," p. 65 (1977).
18. H. F. W. TAYLOR, *J. Appl. Chem.* **10,** 317 (1960).
19. L. S. DENT GLASSER AND F. P. GLASSER, *Acta Crystallogr.* **14,** 818 (1961).
20. L. S. DENT GLASSER, F. P. GLASSER, AND H. F. W. TAYLOR, *Quart. Rev.* **16,** 343 (1962).
21. K. KOYAMA AND Y. TAKÉUCHI, *Z. Kristallogr.* **145,** 216 (1977).